Development of a Hybrid Quantum Chemical and Molecular Mechanics Method with Application to Solvent Effects on the Electronic Spectra of Uracil and Uracil Derivatives

Anders Broo*

Department of Physical Chemistry, Chalmers University of Technology, Göteborg, Sweden

Greg Pearl and Michael C. Zerner*

Quantum Theory Project, University of Florida, Gainesville, Florida 32611

Received: September 26, 1996; In Final Form: December 13, 1996[⊗]

A method for molecular dynamics (MD), Monte Carlo (MC), and energy minimization simulation utilizing a Hamiltonian that is divided into two parts is described. One part is treated with a quantum mechanical Hamiltonian, typically a small part of the simulated system that comprises the chromophore. The other part is treated with a classical mechanical Hamiltonian. This partitioning of the system allows us to simulate, for example, not only electronic spectroscopy but also chemical reactions where a bond is broken or to explore the excited state potential energy surface. The particular choice of the quantum mechanical Hamiltonian, the intermediate neglecting of differential overlap (INDO) model Hamiltonian, also offers the possibility of simulating systems that contain a transition metal, which only rarely have been accessible with traditional MD and MC methods. Test calculations on small systems are presented together with an investigation of the photophysics of uracil and 1,3-dimethyluracil.

I. Introduction

The idea of combining quantum chemical calculations with molecular mechanics is far from new.[1−4] Most previous work has mostly been done using the AM1 or MNDO model Hamiltonians to describe the quantum moiety,[1b−4] as such a simple model allows one to readily examine quite large systems. However, Warshel and co-workers[1a] quite early examined the PPP model Hamiltonian for the quantum moiety. By using the PPP model Hamiltonian for the π-system they were able to simulate excited state properties.

Recently Maseras and Morokuma proposed a hybrid method for geometry optimization where one part of the molecule is described using an *ab initio* quantum chemical method and the remaining part is described with a classical force field.[5] They reported geometries obtained with the hybrid method that deviated very little from geometries obtained with a full *ab initio* calculations.

The previous success of hybrid methods has inspired us to further develop this model. We have chosen the INDO (intermediate neglect of differential overlap) model Hamiltonian for describing the quantum moiety, since we intend to study dynamics of excited states and the importance of the solvent on electronic spectra, and this model is particularly well suited for this purpose. We describe below the implementation of a combined quantum mechanical and molecular mechanical simulation option of the ZINDO quantum chemical program package,[6] which can use either molecular dynamics (MD) or Monte Carlo (MC) algorithms to examine molecular finite temperature properties. By doing a partitioning of the system into two or more pieces both the continuum and the specific solvent interactions can be included in a quantum chemical calculation at an affordable price. Furthermore, since the hybrid method proposed in this work utilizes a semiempirical description of the quantum partitioning, the method is fast enough to enable dynamical processes to be studied. The method developed is then used for studying the photophysics of uracil (U) and 1,3-dimethyluracil (DMU) in different solvents.

Becker and Kogan[7] observed remarkably different luminescence properties for these two species depending on solvent. For instance, in aqueous solution or in an ethanol/methanol solution both U and DMU show weak fluorescence, but in a non-hydrogen-bonding solvent such as 2-methyltetrahydrofuran (2-MTHF) U shows only phosphorescence and no fluorescence while DMU shows only fluorescence and no phosphorescence. Thus, *N*,*N*-dimethyl substitution dramatically changes the potential energy surfaces of the excited state of uracil. The absorption spectra of U and DMU are very similar; the *N*,*N*-dimethyl substitution imposes a blue shift on the position of the band maximum by 3 nm. The spectral shift observed upon changing the solvent from ethanol/methanol to 2-MTHF was found to be negligible.[7] It is well-known that the electronic spectra of most molecules are affected by the solvent. For example, a molecule that has a nonzero dipole moment in the ground state exhibits a shift (red or blue) of the absorption peaks that is proportional to the polarity of the solvent. Traditionally this effect has been described in quantum mechanical calculations by a continuum model.[8] In these models, the solvent is represented as a structureless dielectric that can respond and polarize the dissolved molecule (solute) due to the change in the charge distribution of the solute.

II. Computational Method

II.1. The Model Hamiltonian. The total Hamiltonian, $\mathbf{H}_{tot}$, for the system can be divided into three parts.

$$\mathbf{H}_{tot} = \mathbf{H}_{QM} + \mathbf{H}_{QM/MM} + \mathbf{H}_{MM} \tag{1}$$

where $\mathbf{H}_{QM}$ is the Hamiltonian for the quantum moiety, $\mathbf{H}_{MM}$ is the Hamiltonian for the molecular mechanics moiety, and $\mathbf{H}_{QM/MM}$ is the Hamiltonian that describes the interaction between the quantum moiety and the molecular mechanics moiety. For the remainder of this section we use the following notation: lower case s and s' are used as indices on the classical

[⊗] Abstract published in *Advance ACS Abstracts,* March 1, 1997.

S1089-5639(96)02969-6 CCC: $14.00

atoms, upper case *S* represents the total number of classical atoms. *N* denotes the total number of quantum atoms, lower case *a* and *b* are the indices for quantum atoms, and lower case *i* is the index for electrons. The total energy is then given by eq 2, while eqs 3−5 define terms in eq 2.

$$E_{\mathrm{tot}} = \langle\psi|\mathbf{H}_{\mathrm{QM}} + \mathbf{H}_{\mathrm{QM/MM}}|\psi\rangle/\langle\psi|\psi\rangle + E_{\mathrm{MM}} \tag{2}$$

$$E_{\mathrm{MM}} = \sum_{\mathrm{bonds}} k_{\mathrm{b}}(b_0 - b)^2 + \sum_{\mathrm{angles}} k_\theta(\theta_0 - \theta)^2 + \sum_{\mathrm{dihedral}} k_\varphi(1 - \cos\varphi - \cos 2\varphi - \cos 3\varphi) + \sum_{s}^{S}\sum_{s'>s}^{S} 4\epsilon_{ss'}\left(\frac{\sigma_{ss'}^{12}}{R_{ss'}^{12}} - \frac{\sigma_{ss'}^{6}}{R_{ss'}^{6}}\right) \tag{3}$$

$$\mathbf{H}_{\mathrm{QM}} = -1/2\sum_{i}^{n}\nabla_i^2 + \sum_{i}^{n}\sum_{j>i}^{n}\frac{1}{r_{ij}} - \sum_{i}^{n}\sum_{a}^{N}\frac{Z_a}{r_{ia}} + \sum_{a}^{N}\sum_{b>a}^{N}\frac{Z_a Z_b}{R_{ab}} \tag{4}$$

$$\mathbf{H}_{\mathrm{QM/MM}} = -\sum_{i}^{n}\sum_{s}^{S}\frac{q_s}{r_{is}} + \sum_{a}^{N}\sum_{s}^{S}\frac{Z_a q_s}{R_{as}} + \sum_{a}^{N}\sum_{s}^{S} 4\epsilon_{as}\left(\frac{\sigma_{as}^{12}}{R_{as}^{12}} - \frac{\sigma_{as}^{6}}{R_{as}^{6}}\right) \tag{5}$$

The two last terms in eq 5 are not functions of electronic coordinates and can be treated as an external field that is added to the nuclear repulsion term. In eq 5 we have introduced two new parameters to the force field, the σ_{as} and ϵ_{as}. As a first approximation, the Lennard-Jones parameters used for the MM partitioning were used for the QM/MM interaction. The first term in eq 5, which is a function of electronic coordinates, might be evaluated analytically, or further approximations might be introduced here. Three models for the $1/r_{is}$ interaction were tested. The first model uses analytical evaluation of the $\langle\chi_i|q_s/r_{is}|\chi_i\rangle$ integrals, which arise from the $1/r_{is}$ operator. The second approach calculates the $\langle\chi_i|q_s/r_{is}|\chi_i\rangle$ integrals using an empirical formula, eq 6. In the third approach we calculate the atomic charges q_a, eq 8, in the orthogonalized basis, and replace the two first terms in eq 5 with eq 7. With the latter model we can assume with a good degree of accuracy that the MM partitioning does not interact directly with the quantum electrons and consider $\mathbf{H}_{\mathrm{QM/MM}}$ as a pure classical term. However, a secondary effect arises since the atomic charges are changed during a simulation due to geometry changes.

$$\langle\chi_i|q_s/r_{is}|\chi_i\rangle = \frac{f q_s}{((\zeta/n)^2 + R_{as}{}^2)} \tag{6}$$

$$-\sum_{i}^{n}\sum_{s}^{S}\frac{q_s}{r_{is}} + \sum_{a}^{N}\sum_{s}^{S}\frac{Z_a q_s}{R_{as}} = \sum_{a}^{N}\sum_{s}^{S}\frac{q_a q_s}{R_{as}} f \tag{7}$$

$$q_a = Z_a - \sum_{\mu\in A} P_{\mu\mu} \tag{8}$$

In eq 6, *n* denotes the principal quantum number of the atomic orbital *i*, and ζ is the corresponding exponent, and *f* is a scaling factor; ζ/n is the analytic expression for $\langle\chi_i|q_s/r_{is}|\chi_i\rangle$ over Slater-type orbitals.

Field et al.[1b] tried to use the analytical evaluated $\langle\chi_i|q_s/r_{is}|\chi_i\rangle$ integrals in their AM1/MM model and reported that the interaction energy and the forces were proportionately too large. They chose to evaluate the electronic part of the QM/MM interaction in a way that resembles the MNDO model for treating electrostatics. In our model the analytical evaluated $\langle\chi_i|q_s/r_{is}|\chi_i\rangle$ integrals do not produce unrealistic interaction energies and forces. The differences in binding energy and geometry obtained for the empirical formula $\langle\chi_i|q_s/r_{is}|\chi_i\rangle$ integrals versus the analytical formula are small. Furthermore, the time saved using the empirical formula is small, so we prefer the analytical formula. The atomic charge model produces geometries similar to those obtained with the analytical evaluated integrals, but binding energies, in general, are smaller. The most consistent results are obtained with the analytical evaluation for the electronic part of the QM/MM interaction term in eq 5. However, binding energies are typically too small and the hydrogen bonds too long. To compensate for this, we developed new van der Waals parameters for the QM/MM interaction terms. To avoid a very time consuming reparametrization for all the different atom types, we apply a scaling scheme to the existing van der Waals parameters used already in the classical force field. Several combinations of scaling factors were tested. The final scaling factors that are used throughout this work are 1.6 for the attractive $1/r^6$ term and 0.75 for the repulsive $1/r^{12}$ term. Ho et al. (HMB) used a different reparametrization scheme for the Lennard-Jones interaction term between the molecular and quantum mechanical moiety.[9] HMB mainly concentrated on the binding energy and introduced a new set of Lennard-Jones parameters for the QM/MM interaction based on energies and geometries obtained from Hartree−Fock/6-31G(d) calculations. HMB then scaled the binding energies from the HF/6-31G(d) calculations by a factor of 1.16 to get what they considered as more realistic binding energies. However, no correction for basis set superposition error (BSSE) or electron correlation was included in the reference. Since we have found these effects large, we re-examined this scaling.

For the solvent−solute simulations periodic boundary conditions are used. The simulated solvent−solute system is enclosed inside a box of dimensions *a*, *b*, and *c*. A molecular based cutoff for the nonbonding interactions is used. This cutoff ensures that all atoms in a molecule interact properly with all other atoms in the same molecule and that all interactions between atoms on different molecules are included if the center of mass of the two molecules are within a specified cutoff distance. A cutoff distance of about 10 Å conserves energy within the specified limits of eqs 10 and 11. The largest energy contribution is due to the Coulombic interactions, which falls off very slowly. In fact, a cutoff distance of approximately 30 Å is necessary to get a negligibly small Coulombic interaction. On average, most of the long-distance Coulombic interactions cancel out due to the molecular based cutoff, since the molecules studied are electronically neutral. For simulations of large charged molecules, as for example DNA or proteins, a more sophisticated method is required to reduce possible error of the calculated properties obtained from a MD or MC simulation. These errors are introduced by neglecting some of the long-range electrostatic interactions. The periodic boundary conditions (PBC) also ensure a constant number of particles and preserve the volume. If any molecule leaves the simulation box, it is replaced by a new molecule (its image) on the opposite side of the box with the same velocity as the molecule that left the box.

The force fields used for the molecular mechanics partitioning in the test cases are the same as used in the paper of Field et al.[1b] The water model used in this work is the simple point charge (SPC) model due to Berendsen et al.[10]

II.2. The Molecular Dynamics Algorithm. The dynamic of the system is assumed to follow classical Newtonian

mechanics. After an examination of several different algorithms we choose to use the eqs of motion as outlined by Beeman.[11]

$$\mathbf{r}(t+\Delta t) = \mathbf{r}(t) + \Delta t\mathbf{v}(t) + [4\mathbf{a}(t)\text{-}\mathbf{a}(t-\Delta t)]\Delta t^2/6 \quad (9)$$

$$\mathbf{v}(t+\Delta t) = \mathbf{r}(t+\Delta t)/\Delta t - \mathbf{r}(t)/\Delta t + [2\mathbf{a}(t+\Delta t) + \mathbf{a}(t)]\Delta t/6 \quad (10)$$

$$\mathbf{a}(t+\Delta t) = [\mathbf{v}(t+\Delta t) - \mathbf{v}(t)]/\Delta t \quad (11)$$

The stability of the integration method is tested by calculating the total energy fluctuation (ΔE) and the root-mean-square fluctuation ($R(\Delta E_{\text{rms}})$).[12]

$$|\Delta E| = \frac{1}{N}\sum_{k=1}^{N}\left|\frac{E(k\Delta t) - E_0}{E_0}\right| \quad (12)$$

where E_0 is the initial total energy of the system and N is the number of time steps (Δt).

$$R(\Delta E_{\text{rms}}) = \Delta E_{\text{total}}^{\text{rms}}/\Delta E_{\text{kin}}^{\text{rms}} \quad (13)$$

where $\Delta E_{\text{total}}^{\text{rms}}$ is the root-mean-square fluctuation of the total energy and $\Delta E_{\text{kin}}^{\text{rms}}$ is that of the kinetic energy. The criteria for a stable integrator is $|\Delta E| \leq 0.001-0.003$ and $R(\Delta E_{\text{rms}}) \leq 0.01$.

In simulations of thermodynamic properties it is convenient to use the canonical ensemble (*NVT*), characterized by a constant number of particles, constant volume, and constant temperature. The temperature is kept constant by a coupling to an external heat bath. The coupling to the external heat bath is done following a scheme originally proposed by Berendsen et al.[13] The coupling to the heat bath is obtained by scaling the velocities **v** with a scaling factor λ.

$$\lambda = 1 + \frac{\Delta t}{2\tau}\left(\frac{T_0}{T} - 1\right) \quad (14)$$

where T_0 is the target temperature, T is the actual temperature given by eq 15, τ is the temperature coupling constant, and Δt is the time step.

$$T(t) = \frac{\sum_i^N m_i v_i^2(t)}{K_{\text{Boltzmann}}(3N-6)} \quad (15)$$

The following is the algorithm used for temperature scaling: (1) Calculate new positions $\mathbf{r}(t+\Delta t)$, according to eq 9. (2) Calculate accelerations $\mathbf{a}(t+\Delta t)$, and velocities $\mathbf{v}(t+\Delta t)$, eqs 11 and 10. (3) Calculate $T(t)$ and λ, eqs 14 and 15. (4) Scale $\mathbf{v}(t+\Delta t)$ by λ. (5) Calculate total energy $E_{\text{tot}}(t+\Delta t)$, kinetic energy $E_{\text{kin}}(t+\Delta t)$, and $T(t+\Delta t)$.

A coupling constant τ of 0.7 ps was found to be sufficient to ensure good energy conservation in accordance with eqs 12 and 13.

II.3. The Monte Carlo Algorithm. The Monte Carlo algorithm implemented in the ZINDO program package follows the method outlined by Metropolis et al.[14] The MC simulation is started from an arbitrary configuration. A new configuration is generated by randomly moving each coordinate according to

$$X_{\text{new}} = X_{\text{old}} + a^*\zeta_1 \quad (16)$$

In eq 16, a^* is the maximum allowed displacement and ζ_1 is a random number between -1 and 1. X_{old} and X_{new} are Cartesian coordinate components of an atom. The change in energy ($\Delta E = E_{\text{NEW}} - E_{\text{OLD}}$) is calculated. If ΔE is less than zero, the new configuration is accepted. If ΔE is larger than zero, the new configuration is accepted if $\exp(-\Delta E/RT) > \zeta_2$, where ζ_2 is a random number between 0 and 1. If the new configuration is not accepted, we return to the old configuration and count that as the new configuration. Ensemble averages for any given property F are calculated from

$$\langle F\rangle_{\text{ensemble}} = \frac{1}{M}\sum_{j=1}^{M} \quad (17)$$

This sampling scheme chooses configurations with an $\exp(\Delta E/RT)$ probability, which corresponds to the canonical enable (constant N,V,T).

II.4. Geometry Optimization. Since the gradients are required for the dynamics simulations, they are also available for geometry optimization utilizing any of the gradient-driven methods[16] available in the ZINDO program package.[1]

TABLE 1: New β Parameters for the INDO Model Hamiltonian

atom	β_s (eV)	β_p (eV)
H	−12.6	−1
C	−26.0	−16.32
N	−26.0	−32.94
O	−35.0	−40.0

III. Structural Results

III.1. The INDO Model. A minimum requirement for a computation model that is devoted to studying questions about structure is that the model is capable of reproducing the geometry of the basic moieties of the system under consideration. The INDO model as implemented in the ZINDO program has never been truly optimized to reproduce geometries. Here we report a first step to get geometries from the INDO model that agree with the observed experimental geometries for a set of small molecules. The philosophy used is that a small number of "basic units" are used as a "training set" for a partial optimization of the parameters in the INDO model. We have chosen to keep most of the parameters from the original parametrization constant and have varied only the β parameters for H,C,N,O. As in the MNDO, AM1, and PM3 models, we have chosen to assign different β parameters for s-type and p-type orbitals. The final β values are collected in Table 1. The final geometries of the "training set" are summarized in Table 2. The geometries of the "training set" are compared with AM1 and observed geometries as taken from the original reference for the AM1 model.[15] The average difference between the observed and calculated geometrical parameters is about the same for the INDO model as for the AM1 model for these molecules. This result encouraged us to use the INDO model on some larger systems. We selected the four DNA bases; cytosine, thymine, adenine, and guanine, for further study. In Table 3, the important bond lengths of the four DNA bases are compared with AM1 and MP2/6-31G* data.[17] The INDO model reproduce the MP2/6-31G* geometries with satisfactory accuracy and better than the AM1 model. However, it is important to note here that for molecules with large ring strain, such as, for example, furan, the INDO model with this parametrization predicts the ground state geometry to be puckered. Unrealistic geometries most frequently occur for oxygen-containing molecules using this new parametrization.

Another shortcoming of the INDO model Hamiltonian is in the description of hydrogen bonds. For instance hydrogen bond lengths are far too short and the bonding energies are much too

TABLE 2: Summary of the Geometries of the Training Set[a]

molecule		INDO	AM1	observed		INDO	AM1	observed
H_2	H−H	0.686	0.667	0.742				
N_2	N−N	1.098	1.106	1.094				
O_2	O−O	1.096	1.087	1.216				
C_2H_2	C−C	1.226	1.195	1.203	C−H	1.058	1.061	1.060
C_2H_4	C−C	1.344	1.325	1.339	C−H	1.079	1.098	1.086
	H−C−C	1230.0	122.7	121.1				
C_2H_6	C−C	1.494	1.501	1.536	C−H	1.052	1.117	1.091
	H−C−C	111.6	110.7	110.9				
CO	C−O	1.168	1.171	1.128				
CO_2	C−O	1.209	1.189	1.162				
N_2O	N−N	1.120	1.128	1.126	N−O	1.154	1.175	1.186
$(CH_3)_2CO$	C−C	1.487	1.495	1.507	C−O	1.247	1.236	1.222
	C−C−C	116.9	115.5	117.2				
benzene	C−C	1.406	1.395	1.397	C−H	1.082	1.100	1.084
pyrazine	C−C	1.411	1.419		C−N	1.330	1.349	
	C−H	1.083	1.102		N−C−C	122.3		
	C−N−C	116.2	116.7		C−C−H	121.5		
pyridine	N−C_1	1.318	1.347	1.338	C_2−C_3	1.395	1.396	1.394
	C_3−C_4	1.468	1.396	1.392	C_2−H	1.075	1.097	1.086
	C_3−H	1.069	1.096	1.082	C_4−H	1.128	1.100	1.082
pyrrole	C_1−N	1.353	1.391	1.370	C_1−C_2	1.411	1.401	1.382
	C_2−C_3	1.421	1.436	1.417	C_2−H	1.079	1.085	1.077
	C_3−H	1.079	1.089	1.077	N−H	1.025	0.984	0.996
	C_2−C_3−H	126.2	126.8	125.5	C_3−C_2−H	131.6	130.0	130.8

Average Error in Bonds

INDO	0.025
AM1	0.020

Average Error in Angles

INDO	0.8
AM1	1.1

[a] The AM1 and observed geometrical parameters are those cited in the original reference for the AM1 model.[15]

TABLE 3: Comparison of the Bond Lengths for the Heavy Atoms of the Four DNA Bases Cytosine, Thymine, Adenine, and Guanine, As Predicted by INDO, AM1, and MP2/6-31G*[a]

	INDO	AM1	MP2/6-31G*		INDO	AM1	MP2/6-31G*
			Cytosine				
N_1−C_2	1.388	1.438	1.417	C_2−N_3	1.365	1.403	1.379
N_3−C_4	1.317	1.346	1.317	C_4−C_5	1.445	1.466	1.435
C_5−C_6	1.388	1.371	1.358	C_6−N_1	1.343	1.369	1.357
C_2−O_7	1.260	1.246	1.225	C_4−N_8	1.375	1.382	1.369
			Thymine				
N_1−C_2	1.375	1.412	1.386	C_2−N_3	1.369	1.400	1.386
N_3−C_4	1.377	1.407	1.403	C_4−C_5	1.467	1.476	1.462
C_5−C_6	1.379	1.363	1.354	C_6−N_1	1.359	1.378	1.380
C_2−O_7	1.258	1.249	1.225	C_4−O_8	1.255	1.242	1.230
C_5−C_9	1.482	1.474	1.496				
			Adenine				
N_1−C_2	1.345	1.360	1.353	C_2−N_3	1.324	1.353	1.339
N_3−C_4	1.345	1.368	1.343	C_4−C_5	1.440	1.459	1.399
C_5−C_6	1.430	1.436	1.409	C_1−C_6	1.331	1.376	1.341
C_4−N_9	1.362	1.399	1.378	C5−N7	1.365	1.402	1.381
N_7−C_8	1.324	1.342	1.328	C_8−N_9	1.368	1.413	1.372
C_6−N_{10}	1.377	1.369	1.364				
			Guanine				
N_1−C_2	1.364	1.408	1.373	C_2−N_3	1.320	1.359	1.311
N_3−C_4	1.361	1.385	1.366	C_4−C_5	1.433	1.443	1.394
C_5−C_6	1.453	1.420	1.440	N_1−C_6	1.384	1.420	1.430
C_4−N_9	1.355	1.395	1.370	C_5−N_7	1.360	1.395	1.378
N_7−C_8	1.326	1.345	1.324	C_8−N_9	1.370	1.395	1.375
C_6−O_{10}	1.254	1.239	1.225	C_2−N_{11}	1.381	1.410	1.386
average error				INDO	0.017	AM1	0.022

[a] The MP2/6-31G* geometries is form the work by Sponer and Hobza.[17] [b] The average error is defined as the mean difference between the bond lengths predicted at the MP2/6-31G* level of theory and the bond lengths predicted at the INDO and the AM1 level, respectively.

large; see Table 4. One of the aims of the INDO/MM method is to reproduce solvent effects in chemical reactions and in absorption spectroscopy. Thus, it is of great importance to accurately describe hydrogen bonds when comparing to experimental results and/or high-level *ab initio* predictions. The method outlined in the previous section was first tested on some small dimer complexes, where hydrogen bond strengths and the geometries are well-known.

III.2. The Water Dimer. Hydrogen bonding plays a critical role in many chemical reactions both in solution and in

TABLE 4: Summary of the Water Dimer, As Predicted at Different Levels of Theory

	INDO C_s	INDO C_{2v}	INDO cyclic	MM C_s	AM1/MM	MM/AM1	INDO/MM $\sim C_s$	MM/INDO $\sim C_s$	*ab initio* C_s	obsd
H−O···H (Å)	1.31	1.63	2.27	1.74	2.02	1.99	1.89	1.87	1.95[a]	
O···O (Å)	2.33	2.11	2.68	2.75			2.87	2.87	2.91[a]	2.98[c]
angle	178.0			154.0	159.5	169.0	175.4	176.4	175.5[a]	
ΔE (kcal/mol)	26.2	12.8	3.8	6.6	3.3	4.6	3.3	3.0	5.0 ± 0.1[b]	5.4 ±0.5[d]

[a] MP2(FC)/6-311++G(2d,2p) geometry from ref 20a. [b] Feyereisen, M. W.; Feller, D.; Dixon, D. A. Ref 20e. [c] Dyke, T. R.; Mack, K. M.; Muenter, J. S. *J. Chem. Phys.* **1977**, *66*, 498. [d] Curtiss, L. A.; Frurip, D. J.; Blander, M. *J. Chem. Phys.* **1979**, *71*, 2703.

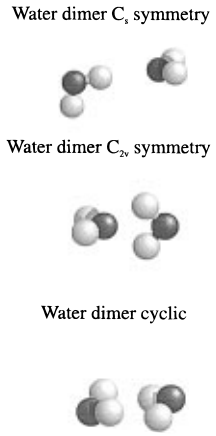

Figure 1. Water dimer geometries.

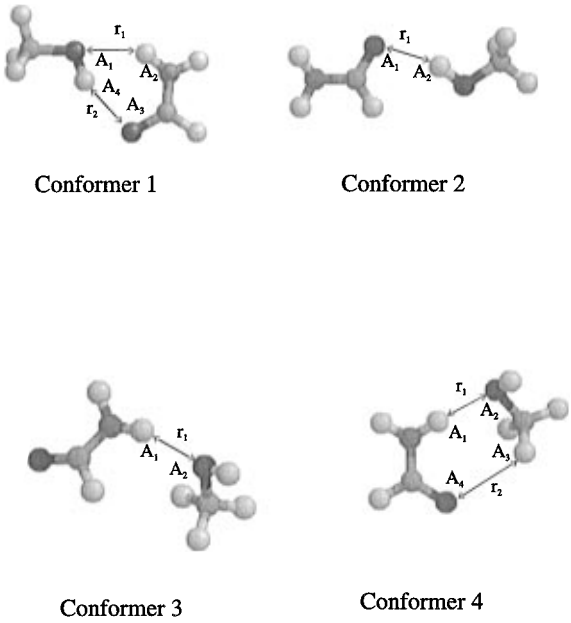

Figure 2. Geometry of the four methanol/formamide conformers discussed in the text. The water/formamide conformers have similar geometries, and the bond distances and bond angles are approximately the same.

biological processes. The water dimer has been used as a model for hydrogen-bonding phenomenon for a long time. It has been investigated in great detail, using classical force fields,[18] semiempirical methods,[15,19] *ab initio* methods including electron correlation,[20] and a hybrid AM1/MM model.[1b] At least three different stable conformers have been identified.[1a,10,15,17,18,20] The most stable conformer has C_s symmetry with one almost linear hydrogen bond. A low energy second conformer possesses C_{2v} symmetry and has two hydrogen bonds, while a third conformer has almost C_{2h} symmetry and possesses three hydrogen bonds. The three lowest energy conformers of the water dimer are displayed in Figure 1. The geometries and hydrogen-bonding energies of the water dimers as predicted by the INDO model and the INDO/MM model are collected in Table 4, along with data from experimental observations and other theoretical predictions. Some care has to be taken when comparing experimental observations and theoretical geometries and bonding energies, since theoretical calculations give bond energies without inclusion of the zero-point vibration energy. Furthermore, the size of the basis set, electron correlation, and basis set superposition have a large effect on the predicted geometries and bonding energies. These effects on the predicted geometry and binding energy of the water dimer were investigated in detail by Frisch et al.[20a] The theoretical predicted geometry with a medium sized basis set, such as 6-31G(d), at the second-order perturbation level (MP2) of theory reproduces the observed experimental geometry well. However, the size of the basis set and electron correlation still have a large impact on the predicted binding energy. In addition, basis set superposition error (BSSE) is also of great importance when calculating binding energies of weakly bonded systems. In a recent detailed study of the water dimer, Feyereisen et al.[20e] estimated the binding energy to 5.0 ± 0.1 kcal/mol. In the study by Feyereisen, very large basis sets were used (up to 547 functions) and the BSSE was carefully examined.

Clearly the INDO model does not reproduce the geometry or the binding energy of the water dimer, as seen in Table 4. The molecular mechanics SPC water model does not reproduce the geometry very well either, although the binding energy and the bulk properties are reasonable well reproduced.[12] The proposed INDO/MM model significantly improves the description of the geometry when compared with either the INDO or MM methods. The binding energy is also significantly improved over the INDO model. The hybrid Hamiltonian proposed in this work produces a more consistent description of the water dimer than does the AM1/MM hybrid Hamiltonian proposed by Field et al.,[1b] as demonstrated by comparison between the QM/MM and MM/QM for each QM model. This notation (X/Y) refers to the first unit (molecule) treated by X, the second unit (molecule) treated by Y, and the interaction through $\mathbf{H}_{QM/MM}$. Although the table summarizes the results of only the lowest energy C_s structure, the C_{2v} and C_{2h} structures are similar.

III.3. The Formamide/Water Complex. The formamide water complex has been studied with theoretical methods by many groups.[20] One of the reasons for the large interest in this complex is that formamide can be considered as the simplest model of a peptide bond. Four conformations have been identified for both the formamide/water and the formamide/methanol complex, all possessing C_s symmetry.[21a] The four energy minima of the two different complexes have very similar geometry. The formamide/methanol complexes, depicted in Figure 2, have corresponding formamide/water analogs. The formamide can act as both a proton acceptor and a proton donor in hydrogen bonding. The two hydrogen bonds formed with water are of almost equal binding strength. However, the carbonyl oxygen binding site (conformer 2) is energetically favored somewhat over the amide hydrogen binding site (conformers 3 and 4). Conformer 1, which has two hydrogen bonds in a cyclic arrangement, was found to be the global energy minimum within the C_s symmetric potential energy surface. The

TABLE 5: Binding Energies and Geometries for the Formamide/Water Complex, in kcal/mol

property	ab initio[a]	MP2/cc-pVDZC$_s$	MP2/cc-pVDZC$_1$	AM1/MM	MM/AM1	INDO/MM	MM/INDO
			Conformer 1				
ΔE	7.8	7.2 (11.8)[b]	6.8 (13.1)[b]	6.7	5.0	7.5	6.4
r_1	2.16	1.96	1.98	2.45	2.07	2.05	2.19
r_2	2.06	1.94	1.93	2.03	2.55	1.84	1.80
A_1(H···O−H)	83.7	84.5	79.2	67.3	84.9	78.8	68.4
A_2(O···H−N)	138.6	139.0	141.3	136.4	160.6	134.5	132.4
A_3(C−O···H)	110.1	105.6	104.9	112.5	112.3	107.9	107.4
A_4(O···H−O)	143.3	146.7	151.4	161.3	126.9	149.8	162.8
			Conformer 2				
ΔE	5.6			5.7	2.9	5.4	3.3
r_1	2.03			2. 12	2.23	1.62	1.70
A_1(C−O···H)	118.8			124.4	141.4	112.0	107.9
A_2(O···H−O)	169.0			175.6	150.0	175.4	174.4
			Conformer 3				
ΔE	5.1			4.0	5,2	4.3	3.6
r_1	2.12			2.01	1.99	1.92	1.95
A_1(N−H···O)	175.9			182.9	176.1	176.2	169.3
A_2(H···O−H)	178.5			182.7	173.3		
			Confomer 4				
ΔE	5.1			5.2	5.2	4.7	3.3
r_1	2.11			2.46	2.03	2.00	1.99
A_1(N−H···O)	177.1			137.8	164.1	144.9	134.9
A_2(H···O−H)	121.5			82.7	109.6		

[a] Reference 21a. [b] Binding energy before BSSE correction.

ab initio potential energy surface was found to be very flat, and in some of the conformers, in Figure 2, large changes in bond angles induce only very small energy changes. Some nonsymmetric points on the full potential energy surface were investigated by Jasien and Stevens,[21a] and they concluded that it was likely that the global energy minimum corresponds to a nonsymmetric geometry. We have used the formamide/water complex as a test case for our model Hamiltonian to allow comparison with Field.[1b] In addition, we have also performed some MP2/cc-pVDZ calculations of the complex in order to estimate the importance of electron correlation on the geometry and the binding energy. One calculation of the MP2/cc-pVDZ was done with C_s symmetry constraints starting from a geometry close to conformer 1. A second geometry optimization was performed without symmetry constraints, starting from the INDO/MM optimized geometry. These calculations suggest that the C_1 symmetric MP2/cc-pVDZ geometry is favored by 1.3 kcal/mol over conformer 1 (C_s). The symmetry breaking leads to a complex that still is cyclic and possesses two hydrogen bonds, but the water molecule has been rotated so that the plane of the water is perpendicular to that of the formamide. However, the binding energy after BSSE correction is smaller for the C_1 symmetric conformer compared to the C_s symmetric conformer. The INDO/MM binding energies and hydrogen bond geometries are collected in Table 5 for comparison. All the INDO/MM optimized geometries are done without symmetry constraints. It is possible to optimize the structures of conformers 1 and 2 preserving a plane of symmetry (C_s) by starting with a planar initial geometry. (The current implementation of INDO/MM does not take advantage of spatial symmetry.) The energies of the complexes of C_s symmetry differ very little from the corresponding ones of C_1 symmetry. The INDO/MM geometries and binding energies are again more consistent than are those obtained from the AM1/MM model. The INDO/MM results compare well with the *ab initio* results and the relative ordering of the stability of the different conformers is reproduced, in contrast to the AM1/MM model. The largest geometry difference between the *ab initio* results and the INDO/MM results is observed when the carbonyl group is a proton acceptor for the hydrogen bond. The O···H bond is calculated too short in all cases by the INDO/MM model. It is likely that this deficiency could be corrected by modifying the Lennard-Jones parameter for the carbonyl oxygen. However, at the present stage we do not want to do a complete reparametrization for every atom type, but rather only use a linear scaling of the MM-MM Lennard-Jones parameter, as discussed previously. Furthermore, the MP2 predicted geometry of conformer 1 has much shorter hydrogen bond lengths than the HF predicted geometry, and it is experiment that we wish our model to reproduce.

III.4. The Formamide/Methanol Complex. The formamide/methanol complex was also studied by Jasien and Stevens.[21a] They reported four low-energy conformations, similar to those found for the formamide/water complex; see Figure 2. The cyclic double-hydrogen-bonded conformer is predicted to be the most stable, as it was in the formamide/water complex. The *ab initio* predicted ordering of the relative stability of the four conformers is not reproduced by either of the hybrid models, but both hybrid models predict the cyclic conformer as the most stable one; see Table 6. Once again, we can see that the INDO/MM model produces more consistent results than does the AM1/MM model.[1b] The INDO/MM binding energies are in most cases larger than the *ab initio* predicted binding energies. The INDO/MM predicted hydrogen bond lengths are generally too short compared to the *ab initio* predicted ones for the formamide/water complex, and too long for the formamide/methanol complex. However, inclusion of electron correlation and use of larger basis sets change the *ab initio* predicted geometries greatly, so a definitive conclusion is hard to draw from the above comparison. In summary, the INDO/MM model reproduces the *ab initio* data reasonably well. Furthermore, the differences between the INDO/MM and MM/INDO results are much smaller than those reported for the AM1/MM and MM/AM1 treatment.[1b] It is also important to remember that the potential energy surfaces for the two systems are very flat around the reported energy minima (both the *ab initio* and INDO/MM surfaces). Thus, relatively large changes in angles and bond lengths make only small changes in the total energy.

TABLE 6: Binding Energies and Geometries for the Formamide/Methanol Complex, in kcal/mol

property	*ab initio*[a]	AM1/MM	MM/AM1	INDO/MM	MM/INDO
		Conformer 1			
ΔE	7.6 (7.8)[b]	6.4	6.1	9.2	11.4
r_1	2.08 (2.17)	2.32	1.97	2.17	2.25
r_2	1.94 (2.05)	2.17	2.42	2.08	2.10
A_1(H···O−H)	85.5 (83.1)			89.6	58.8
A_2(O···H−N)	139.3 (139.3)	139.3	153.7	140.9	122.0
A_3(C−O···N)	109.8 (110.0)	115.0	109.9	113.9	95.7
A_4(O···H−O)	144.1 (144.3)	139.3	128.2	134.3	136.0
		Conformer 2			
ΔE	5.6	5.6	2.9	4.7	6.9
r_1	1.93	2.13	2.32	2.06	2.02
A_1(C−O···H)	173.0	168.3	150.5	174.9	138.1
A_2(O···H−O)	136.3	141,6	97.5	175.0	107.3
		Conformer 3			
ΔE	4.5	3.1	5.6	6.2	4.9
r_1	2.00	1.98	1.91	2.12	2.14
A_1(N−H···O)	174.5	169.9	177.3	141.2	148.1
A_2(H···O−H)	127.3	156.8	125.6	92.4	94.6
		Conformer 4			
ΔE	4.7	2.8	5.8	5.5	7.8
r_1	1.95	2.02	1.93	2.16	1.95
A_1(N−H···O)	176.6	162.1	174.5	148.9	175.5
A_2(H···O−H)	118.4	91.3	108.5	83.2	92.2

[a] HF/DZ geometry optimized, ref 21a. [b] HF/DZP geometry optimized, ref 21a.

IV. Spectroscopic Results

We have developed a model useful for examining the absorption and emission properties of molecules. We now examine the low-energy spectroscopy of uracil and 1,3-dimethyluracil, one of several motivations for this work.

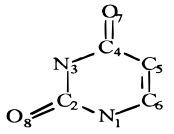

Uracil(U)

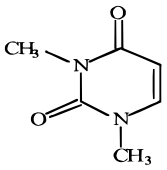

1,3-dimethyluracil(DMU)

It has been shown by Becker and Kogan[7] that the character of the luminescence of U and DMU is different depending on the solvent. Both U and DMU fluoresce in polar hydrogen-bonding solvents (protic), but only DMU shows fluorescence in polar non-hydrogen-bonding solvents (aprotic) and U only phosphoresces in the latter type of solvents. Baraldi et al.[23] have conducted a theoretical study of the spectroscopy of U and several uracil derivatives using an INDO-based method called CS-INDO. The observed absorption spectra of uracil were well reproduced, and the photophysics were discussed. However, they did not include solvent interactions in the description and did not address the dependency of the emission on the solvent.

In a previous classical molecular dynamics study one of us investigated the DMU complex in water solution.[24] The MD simulation showed that each carbonyl oxygen of DMU accepts protons via hydrogen bonding with at least two water molecules. The binding strength was not computed, but the carbonyl oxygen with one neighboring CH_3 group (O_7) bound a water molecule considerably more tightly than did the other carbonyl oxygen, O(8). We have performed MD simulations on uracil and DMU with 98 water molecules using the INDO/MM hybrid. The water molecules were included in the MM moiety, and U (or DMU) was treated as the quantum system. Periodical boundary conditions were used, and the simulated system was enclosed in a 16 × 16 × 16 Å box. The system was first equilibrated at 77 K by a combination of geometry optimization and MD simulations with high-friction temperature scaling λ to remove all excess energy from the arbitrary initial structure. After equilibration the system was run for 4 ps, requiring about 6 h of CPU time on an IBM RS6000/590 workstation. The hybrid MD simulation of the U−water system predicts a hydrogen-bonding pattern similar to that of the all classical MD simulation of the DMU−water system. In Figures 3 and 4 the hydrogen bond distances between the two carbonyl oxygens and the neighboring water molecules are plotted as a function of simulation time. The carbonyl oxygen with only one neighboring N−H group has two water molecules that are strongly hydrogen bonded during most of the simulation, Figure 3. At the end of the simulation a third water molecule collided with one of the hydrogen-bonded water molecules and exchanged position with the "permanent" water molecule close to the carbonyl oxygen. The second hydrogen binding site is less crowded during the simulation, Figure 4. The difference in binding capability between the two sites was more pronounced in the pure classical MD simulation of DMU in water.[24] Clearly at least one water molecule is stationary in the vicinity of the carbonyl oxygens of both U and DMU, at least during the time of our simulation.

To investigate the solvent effect on the absorption spectrum of U and DMU several INDO/S-CIS calculations were performed. In all of these spectra calculations the simulation geometries determined by the INDO/1 moiety were used, unless otherwise stated in Table 7 or 8. The absorption spectra were obtained from configuration interaction (CI) calculations, which involved all of the single excited configuration state functions that have $\pi \rightarrow \pi^*$ and $n \rightarrow \pi^*$ character (CIS). The absorption spectrum predicted by the INDO/S-CIS model, in vacuum, agrees very well with the spectrum previously published by Baraldi et al.[23] using a slightly different parametrization of the INDO model (CS-INDO).The effectiveness of the INDO/s model in reproducing the spectra of nucleotides is well documented.[25] The predicted absorption spectra of U and DMU in vacuum and in water solution are compared with the observed absorption spectra in Tables 7 and 8. The solution spectra were computed using the traditional SCRF model using a spherical

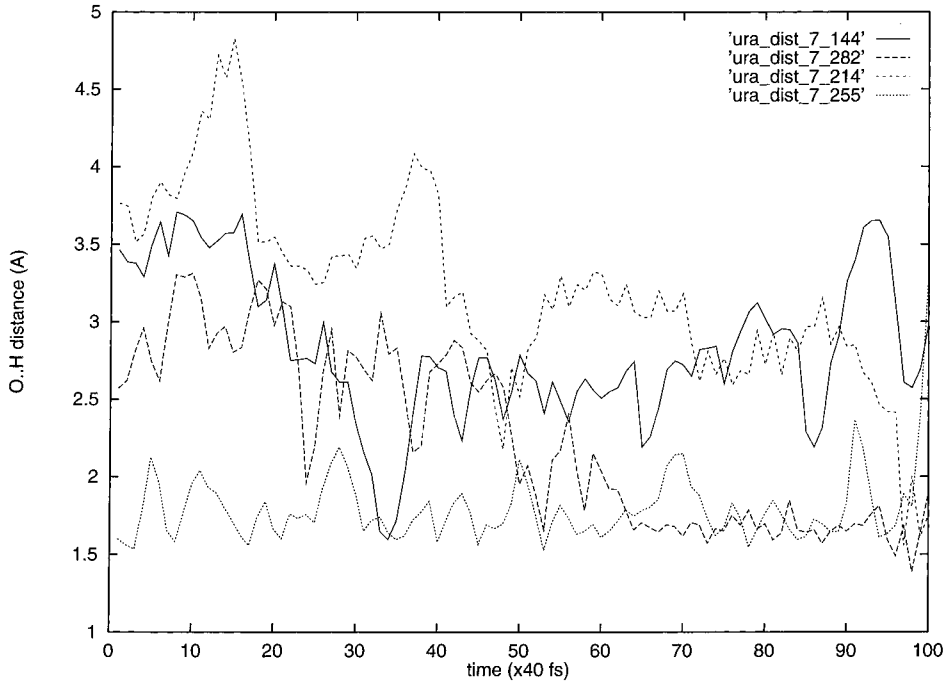

Figure 3. Hydrogen bond distance between the O_7 carbonyl and the neighboring water hydrogen's as a function of simulation time.

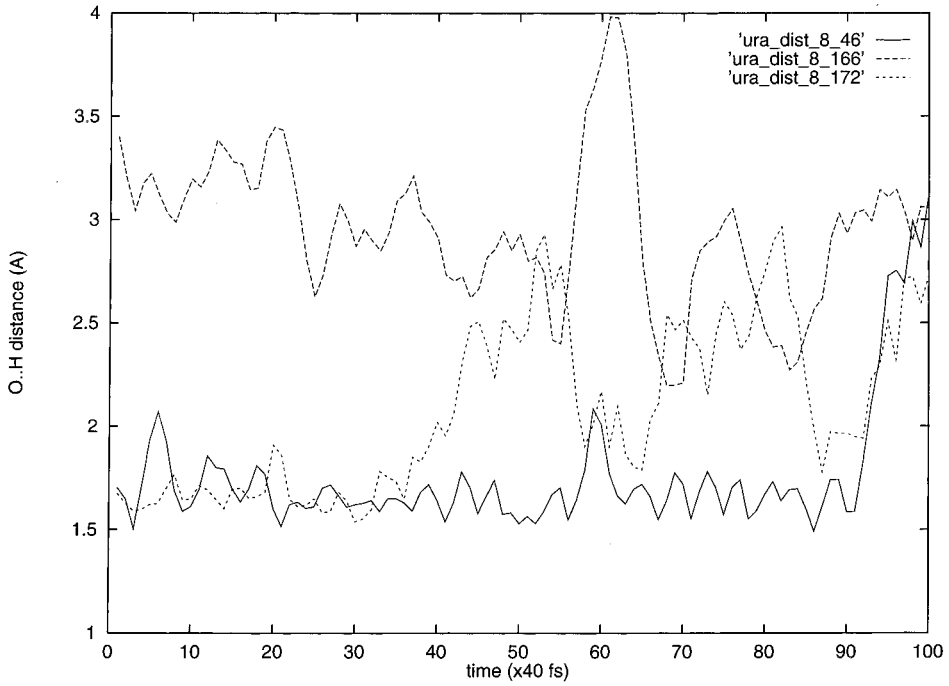

Figure 4. Hydrogen bond distance between the O_8 carbonyl and the neighboring water hydrogen's as a function of simulation time.

cavity.[8] Since the SCRF model does not include specific solvent interactions, we also computed the absorption spectra of U and DMU in the presence of eight water molecules. In the spectral calculation the water molecules were represented by the point charges from the classical force field. We geometry optimize both a U and a DMU complex with four water molecules surrounding each carbonyl oxygen using the INDO/MM model and the BFGS procedure.[14] For both molecular complexes one water molecule was found to be hydrogen bonded to each carbonyl oxygen (O−H) at a distance of about 1.65 Å. Then the remaining water molecules form a second solvation shell around the most tightly bound water molecule. In the U + $8H_2O$ complex one water molecule forms a cyclic configuration with one hydrogen bond to O_7 and a second hydrogen bond to the N_3 hydrogen. This type of cyclic double-hydrogen-bonded complex cannot be formed with DMU and water. In this loosely bound system several energy minima are possible, and the above described geometry is just one of the many close lying conformers. The water structure around the carbonyl groups is similar for both U and DMU. The predicted spectra of these complexes are also found in Tables 7 and 8. All theoretical investigations predict the lowest state to have $n \rightarrow \pi^*$ character, in agreement with the interpretation of the emission spectra reported by Becker et al.[7] and the supersonic jet spectrum of uracil reported by Fujii et al.[27]

Fujii observed two band systems, one with the 0^0 transition located at 35 288 cm^{-1} (system I) and one system with the 0^0 transition located at 30 917 cm^{-1} (system II). The vibration progression of system I was found to be very similar to the ground state vibration spectrum, while the vibration progression

TABLE 7: Comparison of Predicted Absorption Spectra of Uracil with Observed Spectra; A Recent Published *ab initio*, CASPT2, Predicted Spectrum Is Also Listed;[26] Transition Energies Are Given in cm^{-1}/1000 and Numbers in Parentheses Are Oscillator Strengths

	INDO	INDO + SRCF	INDO U + 8H_2O	INDO U + 8H_2O + SCRF	CS-INDO ref 23	CASPT2 ref 26	obsd
n → π^*	32.3 (0.0008)	33.0 (0.0008)	33.2 (0.0009)	33.2 (0.0009)	32.7 (0.001)	36.6 (0.0002)	35.3[a]
n → π^*	38.4 (0.0000)	38.4 (0.0008)	39.1 (0.0004)	38.7 (0.0146)	39.6 (0.000)	48.4 (0.0000)	41.7?[b,c]
π → π^*	40.7 (0.39)	40.3 (0.39)	40.3 (0.38)	40.1 (0.36)	42.6 (0.34)	40.3 (0.19)	38.2[c]
π → π^*	48.8 (0.20)	47.4 (0.21)	48.0 (0.21)	48.1 (0.20)	50.4 (0.19)	46.9 (0.08)	46.5[c]
n → π^*	50.2 (0.0002)	50.6 (0.0002)	50.4 (0.0008)	50.3 (0.0052)	*d*	51.4 (0.0000)	*d*
? π → σ^*	51.4 (0.0003)	52.2 (0.0004)	52.2 (0.0005)	52.0 (0.0133)	*d*	*d*	*d*
π → π^*	52.5 (0.08)	53.5 (0.11)	53.0 (0.10)	53.2 (0.11)	52.2 (0.47)	52.1 (0.29)	51.3[c]
n → π^*	55.5 (0.0007)	54.7 (0.0012)	56.1 (0.0035)	56.3 (0.0064)	*d*	56.1 (0.0001)	
π → π^*	56.8 (0.17)	56.5 (0.02)	56.4 (0.10)	56.3 (0.03)	57.1 (0.10)	56.5 (0.76)	56.5[c]
^{3}(π → π^*)	15.9	16.6	16.1	16.0	24.4	*d*	22.2[e]
^{3}(n → π^*)	29.2	30.8	30.1	30.2	30.6	*d*	*d*

[a] Electronic spectra of uracil in a supersonic jet.[27] [b] CD spectra of dioxyuracil monophosphate in water solution.[28] [c] Uncertain assignment from the CD measurements.[28] [d] This transition was not reported in the cited work. [e] Reported as phosphorescence in 2-MTHF solution at 77 K.[7]

TABLE 8: Comparison of Predicted Absorption Spectra of 1,3-Dimethyluracil with Observed Spectra; Transition Energies Are Given in cm^{-1}/1000 and Numbers in Parentheses Are Oscillator Strengths

	INDO	INDO + SRCF	INDO DMU + H_2O	INDO DMU + 8H_2O +SCRF	CS-INDO ref 23	obsd
n → π^*	30.7 (0.0009)	31.3 (0.0009)	30.8 (0.0006)	31.8 (0.0009)	31.7 (0.000)	35.3[a]
n → π^*	37.3 (0.0001)	37.3 (0.0005)	35.5 (0.0013)	37.2 (0.0068)	38.5 (0.000)	41.7?[b,c]
π → π^*	39.6 (0.32)	39.0 (0.33)	37.4 (0.31)	38.2 (0.32)	41.4 (0.28)	37.7[e]
π → π^*	47.8 (0.20)	46.7 (0.21)	44.3 (0.23)	46.0 (0.22)	48.1 (0.16)	46.5[c]
π → π^*	48.0 (0.11)	48.7 (0.13)	47.5 (0.21)	49.1 (0.14)	50.6 (0.46)	
n → π^*	49.4 (0.0008)	49.6 (0.0003)	49.6 (0.0005)	49.5 (0.0006)	*d*	*d*
?π → σ^*	50.8 (0.0002)	51.5 (0.0002)		51.5 (0.0045)	*d*	*d*
π → π^*	53.2 (0.41)	53.7 (0.35)	51.3 (0.29)	53.6 (0.38)	54.4 (0.39)	51.3[c]
n → π^*	54.6 (0.0003)	53.8 (0.0002)	53.4 (0.0029)	55.2 (0.0080)	*d*	*d*
π → π^*	58.3 (0.06)	56.4 (0.03)	55.1 (0.08)	55.7 (0.07)	61.1 (0.11)	56.5[c]
^{3}(π → π^*)	17.2	17.6	16.2	16.4	24.4	*d*
^{3}(n → π^*)	27.6	28.4	28.8	29.0	29.6	*d*

[a] Electronic spectra of uracil in a supersonic jet.[27] [b] CD spectra of dioxyuracil monophosphate in water solution.[28] [c] Uncertain assignment from the CD measurements.[28] [d] This transition was not reported in the cited work. [e] Absorption spectrum of DMU recorded in 2-MTHF solution at 77 K.[7]

for system II was very different. The 35 288 cm^{-1} peak was assigned as n → π^* and the 30 917 cm^{-1} peak was assigned to be an n → π^* transition from a different tautomeric form of uracil. Fujii assigned the latter transition to be from the 2-enol tautomer based on an early *ab initio* calculation of the relative stability of the possible enol−keto tautomers of uracil, even though the suggested tautomer was calculated to be 72.1 kJ/mol less stable than the 2,4-diketo tautomer. Recently more sophisticated calculations of the relative stability of the different uracil tautomers have been reported.[29] The conclusion from the latter works is clear: only the 2,4-diketo tautomer of uracil is expected. The next most stable tautomer is calculated less stabilized relative to the 2,4-diketo tautomer by 45 kJ/mol. A tempting alternative assignment of the two n → π^* peaks would be that both originate from the 2,4-diketo tautomer, and this reassignment is in reasonably good agreement with the INDO/S-CI and CS-INDO calculations. However, the CASPT2 predicted spectrum of uracil[24] would then be in error by about 0.6 eV for the n → π^* transitions. By inspection of the molecular orbitals (MO) from the INDO calculations two nonbonding MOs are identified. In both U and DMU the highest occupied nonbonding MO is slightly localized on the O_7 carbonyl group, and the other occupied nonbonding MO is slightly localized at the other carbonyl group. Excitations from these two MOs will result in at least two low lying n → π^* transitions, which also is predicted by all calculations. All emission studies of uracil and uracil derivatives suggest that an n → π^* state is the lowest emitting state.[7,27,30]

In general, the emitting state is the lowest exited state of a given multiplicity, and this state is relaxed with respect to solvent and geometric parameters. Thus, we have to estimate the geometry of the lowest exited state to be able to calculate the emission spectra of U and DMU. We have optimized the lowest excited state geometry of U by calculating the lowest open shell singlet using the ROHF formalism.[31] Only small changes in geometry are found comparing the 2 ^{1}A″ state and 1 ^{1}A″. The C_4-O_7 bond length is increased in the 2 ^{1}A″ state, and there is a corresponding decrease of the C_4-C_5 bond length and increase of the C_5-C_6 bond length. The C_4-O_7 bond length suggests single-bond character in the 2 ^{1}A′ state. Furthermore, the carbonyl oxygen bends toward the N_3 hydrogen. These geometric changes suggest that a proton transfer might be favored in the excited state. If the proton transfer occurs, the emission could take place from two different tautomers. The proton transfer mechanism might offer an explanation of the two systems of bands observed in the supersonic jet fluorescence excitation spectrum reported by Fujii et al.[27] The lowest n → π^* state of the 4-enol tautomer is located at about 34 900 cm^{-1}, which is slightly blue shifted with respect to the lowest n → π^* transition of the 2,4-diketo tautomer, Figure 5. The lowest π → π^* transition of the 4-enol tautomer is calculated at 35 000 cm^{-1}. Clearly, this spectrum does not agree well with the observed spectrum recorded in the supersonic jet. The λ_{max} of the fluorescence of U, using the optimized excited state geometry, is predicted to be at ∼29 000 cm^{-1} in vacuum and at ∼30 200 cm^{-1} in water solution using the SCRF model. The observed λ_{max} for the fluorescence is 33 333 cm^{-1} in 2-MTHF and ethanol/methanol at 77 K[7] and 31 350 cm^{-1} in water solution,[29] and the lowest triplet state of both U and DMU has π → π^* character. The ^{3}(π → π^*) state is predicted at much

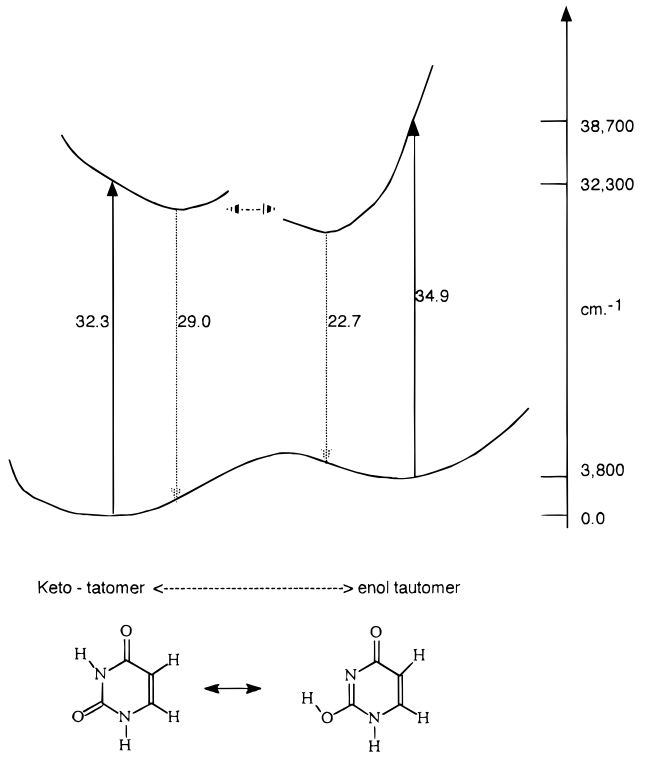

Figure 5. Schematic drawing of the keto−enol tautomerization. The energies of the excitations are from CIS calculation, and the keto−enol separation in the ground state of 3800 cm^{-1} is from the *ab initio* calculations of ref 29. The INDO/1 SCF calculations do not give barriers, but suggest that both keto and enol forms have real minima in both ground and excited states.

lower energy compared to what is observed for the phosphorescence of U in 2-MTHF solution. The $^3(\pi \rightarrow \pi^*)$ state is slightly blue shifted by the solvent, but the predicted transition energy is still far from the observed phosphorescence energy.[32]

Let us now turn the focus upon the photophysics of the two molecules. It is commonly believed that if two states are close in energy, then vibrational coupling between the two states is facilitated and the luminescence will be effected.[33] From Tables 7 and 8 it is clear that the second $n \rightarrow \pi^*$ state is predicted to be close in energy to the first $\pi \rightarrow \pi^*$ state. The energy separation of these two states is predicted to be 2300 cm^{-1} for both U and DMU in vacuum. In water solution (SCRF) the state separation is decreased to 1900 cm^{-1} for U and 1700 cm^{-1} for DMU. With both reaction field and specific solvent interactions the energy splitting is 1400 cm^{-1} for U and 1000 cm^{-1} for DMU. Solvent interaction narrows the state energy difference considerably. Thus, we expect that vibrational motions of the skeleton will cause state mixing and offer an effective radiationless deactivation channel for both molecules. Furthermore, this deactivation channel will be as likely for both U and DMU in both types of solvents. To confirm the state-mixing mechanism for the deactivation, we has computed the absorption spectrum of DMU using 10 geometries obtained during the MD simulation of DMU and the surrounding water molecules. The predicted spectrum is depicted in Figure 6. Around 35 000 cm^{-1} a weak band appears in the predicted spectrum. By inspection of the CI eigenvectors the intensity increase of the $n \rightarrow \pi^*$ is due to mixing of the close lying $\pi \rightarrow \pi^*$ state. The vibrational mode responsible for the mixing is an out-of-plane bending mode of the O_7 carbonyl group. Our results are in good accord with the observed very low quantum yield for the fluorescence. However, the reason for the absence of fluorescence and the large quantum yield for the phosphorescence for U in non-hydrogen-binding solvents is not explained by the above discussion. One possible explanation is that the N_3 proton is transferred to the O_7 carbonyl oxygen in the excited state of U, Figure 5. This proton transfer is blocked by a strong hydrogen bond between the solvent and U in hydrogen-bonding solvents. This type of proton transfer in the excited state is not possible for DMU. We predict the lowest triplet state of the 4-enol tautomer to be at 17 100 cm^{-1} and with $^3(\pi \rightarrow \pi^*)$ character, which still is about 5000 cm^{-1} lower in energy than that observed. In the work by Becker and Kogan[7] the possible tautomerism was discussed, but their final conclusion was that the difference in photophysical behavior for U and DMU most likely was due to different microsolvent

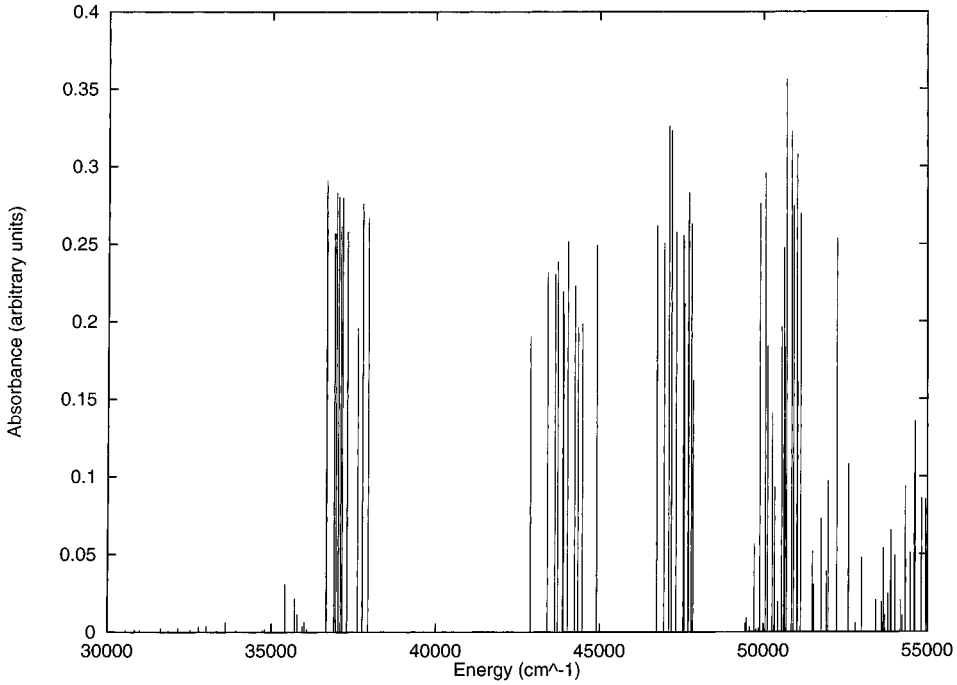

Figure 6. INDO/S-CIS predicted spectrum of 1,3-dimethyluracil using 10 geometries taken from a 4 ps long MD simulation with a time separation of 0.4 ps.

environment. The present study confirms that the solvation shell is different around U compared to DMU, but the difference is small and the effect on the calculated absorption spectrum is small.

V. Summary

A hybrid method that combines a quantum mechanical and a molecular mechanical description of a molecular system is presented. This new method utilizes the INDO model Hamiltonian for the quantum moiety. The INDO model Hamiltonian is parametrized for almost every element of the periodical table, in contrast to the AM1 model, which is the most frequently used model Hamiltonian for the quantum moiety in earlier hybrid methods.[1b−4] Furthermore, with the INDO model as implemented in the ZINDO program package it is possible to do RHF, UHF, PUHF, and ROHF (with both low-spin and high-spin coupling) calculations. Thus, a very flexible hybrid method is developed. Observed and *ab initio* computed geometries and binding energies of hydrogen-bonding complexes are reproduced with the INDO/MM model as accurately as the AM1/MM model.[1b] The INDO/MM model proposed here provides a more consistent description of the hydrogen-bonded complexes than does the AM1/MM model, confirmed by the observation that the results are less sensitive to the partitioning between the classical and quantum partitions.

The method is then used to investigate the dynamics and photophysics of uracil and 1,3-dimethyluracil in protic and aprotic solvents. The molecular dynamics simulation and geometry optimization of uracil and 1,3-dimethyluracil in water solution demonstrated that at least one water molecule is tightly bound to each of the two carbonyl oxygen atoms. The low quantum yield for fluorescence is due to quenching by vibrational induced state mixing between one $n \rightarrow \pi^*$ and one $\pi \rightarrow \pi^*$ state that are predicted to be very close in energy in both molecules. The deactivation vibrational mode is an out-of-plane bending of the O_7 carbonyl oxygen. In a non-hydrogen-bonding solvent uracil has a much larger quantum yield for phosphorescence than for fluorescence, while 1,3-dimethyluracil shows only fluorescence in any type of polar solvent. Since the dynamics of the two systems seems to be more or less the same, we suggest that the initial state for the phosphorescence is the 4-enol tautomer of uracil. The 4-enol uracil is obtained by an internal proton transfer in the excited state that might be blocked by a hydrogen-bonded solvent molecule in hydrogen-binding solvent.

Acknowledgment. This work has been supported in part by The Swedish Natural Science Research Council (NFR), the Office of Naval Research (ONR), and Natural Science Foundation (NSF) through Grant CHE-9312651.

References and Notes

(1) (a) Warshel, A.; Levitt, M. *J. Mol. Biol.* **1976**, *103*, 227. (b) Field, M. J.; Bash, P. A.; Karplus, M. *J. Comput. Chem.* **1990**, *6*, 700. (c) Singh, U. C.; Kollman, P. A. *J. Comput. Chem.* **1986**, *7*, 718.

(2) (a) Gao, J. *J. Phys. Chem.* **1992**, *96*, 537. (b) Gao, J.; Pavelites, J. J. *J. Am. Chem. Soc.* **1992**, *114*, 1912. (c) Gao, J.; Xia, X. *Nature* **1992**, *258*, 631. (d) Gao, J, *J. Am. Chem. Soc.* **1993**, *115*, 2930. (e) Gao, J. *J. Am. Chem. Soc.* **1995**, *117*, 8600.

(3) Liu, H.; Müller-Plathe, F.; van Gunsteren, W. F. *J. Chem. Phys.* **1995**, *102*, 1722.

(4) Thompson, M. A. *J. Phys. Chem.* **1995**, *99*, 4794.

(5) Maseras, F.; Morokuma, K. *J. Comput. Chem.* **1995**, *16*, 1170.

(6) ZINDO, a semiempirical program package. Zerner, M. C. Univesity of Florida, Gainesville, FL 32611.

(7) Becker, R. S.; Kogan, G. *Photochem. Photophys.* **1980**, *31*, 5.

(8) Karelson, M. M.; Zerner, M. C. *J. Phys. Chem.* **1992**, *96*, 6949

(9) Ho, L. L.; MacKerell, A. D.; Bash, P. A. *J. Phys. Chem.* **1996**, *100*, 4466.

(10) Berendsen, H. J. C.; Postma, J. P. M.; van Gunsteren, W. F.; Hermans, J. In *Intermolecular Forces*; Pullman, B., Ed.; Reidel: Dordrecht, Holland, 1981; p 331.

(11) Beeman, D. *J. Comput. Phys.* **1976**, *20*, 130

(12) Watanabe, M.; Karplus, M. *J. Chem. Phys.* **1993**, *99*, 8063.

(13) Berendsen, H. P. C.; Postma, J. P. M.; van Gunsteren, W. F.; DiNola, A.; Haak, R. J. *J. Chem. Phys.* **1984**, *81*, 3684.

(14) Metropolis, N.; Rosenbluth, A. W.; Rosenbluth, M. N.; Teller, A. H.; Teller, E. *J. Chem. Phys.* **1953**, *21*, 1087.

(15) Dewar, M. J. S.; Zoebisch, E. G.; Healy, E. F.; Stewart, J. P. *J. Am. Chem. Soc.* **1985**, *107*, 3902.

(16) (a) Head, J. D.; Zerner, M. C. *Chem. Phys. Lett.* **1986**, *131*, 359. (b) Head, J. D.; Zerner, M. C. In *Adv. Quantum Chem.* **1988**, *20*, 239. (c) Head, J. D.; Weiner, B.; Zerner, M. C. *Int. J. Quantum Chem.* **1988**, *33*, 177.

(17) Sponer, J.; Hobza, P. *J. Phys. Chem.* **1994**, *98*, 3161

(18) Jorgensen, W. L.; Chandrasekhar, J.; Madura, J. D.; Impey, R. W.; Klein, M. L. *J. Chem. Phys.* **1983**, *79*, 926.

(19) Stewart, J. J. P. *J. Comput. Chem.* **1985**, *10*, 3902.

(20) (a) Frisch, M. J.; DelBene, J. E.; Binkley, J. S.; Schaefer, H. F., III. *J. Chem. Phys.* **1986**, *84*, 2279. (b) Mezei, M.; Dannenberg, J. J. *J. Phys. Chem.* **1988**, *92*, 5860. (c) Marsden, C. J.; Smith, B. J.; Pople, J. A.; Schaefer, H. F., III.; Radom, L. *J. Chem. Phys.* **1991**, *95*, 1825. (d) Feller, D. *J. Chem. Phys.* **1992**, *96*, 6104. (e) Feyereisen, M. W.; Feller, D.; Dixon, D. A. *J. Phys. Chem.* **1996**, *100*, 2993.

(21) (a) Jasien, P. G.; Stevens, W. J. *J. Chem. Phys.* **1986**, *84*, 3271. (b) JContador, J. C.; Sanchez, M. L.; Aguilar, M. A.; del Valle, F. J. O. *J. Chem. Phys.* **1996**, *104*, 5539, and references therein.

(22) Weiner, S. J.; Kollman, P. A.; Nguyen, D. T.; Case, D. A. *J. Comput. Chem.* **1986**, *7*, 230.

(23) Baraldi, I.; Bruni, M. C.; Costi, M. P.; Pecorari, P. *Photochem. Photophys.* **1990**, *52*, 361.

(24) Broo, A. *Chem. Phys.* **1993**, *174*, 127.

(25) (a) Callis, P. R. *Annu. Rev. Phys. Chem.* **1983**, *34*, 329. (b) Callis, P. R. *Photochem. Photobiol.* **1986**, *44*, 315. (c) Broo, A.; Holmen, A. Submitted.

(26) Lorentzon, J.; Fülscher, M. P.; Roos, B. O. *J. Am. Chem. Soc.* **1995**, *117*, 9265.

(27) Fujii, M. T.; Tamura, T.; Mikami, N.; Ito, M. *Chem. Phys. Lett.* **1986**, *126*, 583.

(28) Sprecher, C. A.; Johnson, W. C. *Biopolymers* **1977**, *16*, 2243.

(29) (a) Gould, I. R.; Burton, N. A.; Hall, R. J.; Hillier, I. H. *J. Mol. Struct. (THEOCHEM)* **1995**, *331*, 147. (b) Estrin, D. A.; Paglieri, L.; Corongiu, G. *J. Phys. Chem.* **1994**, *98*, 5653.

(30) Williams, S. A.; Renn, C. N.; Callis, P. R. *J. Phys. Chem.* **1987**, *91*, 2730.

(31) (a) Edwards, W. D.; Zerner, M. C. *Theor. Chim. Acta* **1987**, *72*, 347. (b) Roothaan, C. C. *J. Rev. Mod. Phys.* **1960**, *32*, 179.

(32) Ridley, J. E.; Zerner, M. C. *Theor. Chim. Acta* **1976**, *42*, 223.

(33) Lim, E. C. *J. Phys. Chem.* **1986**, *90*, 6770.